# Robust $\mathcal{H}_\infty$ Controller Synthesis for Hovering Ducted-Fan VTOL Micro-UAV

Naoki Sean Pross *

***Abstract*—This paper models an experimental vertical take-off landing (VTOL) micro unmanned aerial vehicle (UAV) device developed at the University of Applied Sciences OST RJ in Rapperswil. The model is then converted to a linear time invariant (LTI) state space plant to design a robust controller using $\mathcal{H}_\infty$ synthesis that tracks a piecewise constant spatial position reference. In conclusion simulated preliminary results on the controller performance are presented.**

## I. Introduction

The presented VTOL micro UAV is a device developed by T. Rothlin [1] at the University of Applied Sciences OST RJ, Rapperswil that can be steered only by controlling the propeller velocity and the angle of attack of four flaps under the ducted fan. Currently there is not a control algorithm for the UAV and the uncertainties from aerodynamics and gyroscopic effects caused by the propeller make this an interesting candidate for robust controller synthesis.

### A. Related Works

A previous prototype of the device [2] had been controlled with a set of decoupled PI controllers for axial and vertical control, which allowed the UAV to hover albeit non-robustly. Similar devices are presented in [3, 4] with a similar decoupled approaches using a linearization in the latter and backstepping techniques in the former, in both robustness is not built into the controller design but rather tested afterwards.

Finally [5] and [6], analyze devices that are very similar to the presented UAV. The former approaches the problem using a combination of PID with non-linear techniques, while the latter uses μ-synthesis and $DK$ iteration to synthesize a robust controller. As done in the present work [6] uses uncertainty block to compensate for inaccuracies in the aerodynamics modelling, as well as errors caused by the linearization.

### B. Organization

Section II presents a derivation of a model for the plant, and then §III illustrates the controller design. Finally, in §IV the closed loop design is simulated and briefly discussed.

## II. System Modelling

### A. Reference Frames

To model the dynamics of the ducted-fan UAV two reference frames are required: an inertial frame and a body-frame attached to the center of mass [7]. In the inertial frame we work in the base given by the unit vectors $\{\hat{\imath}, \hat{\jmath}, \hat{\mathbf{k}}\}$, whereas in the body-frame we use $\{\hat{\mathbf{x}}, \hat{\mathbf{y}}, \hat{\mathbf{z}}\}$ together with the Euler angles $\boldsymbol{\Theta} = [\phi\ \vartheta\ \psi]^\mathsf{T}$. The angular velocity $\boldsymbol{\Omega} = [p\ q\ r]^\mathsf{T}$ is then related to $\boldsymbol{\Theta}$ by

$$\dot{\boldsymbol{\Theta}} = \begin{bmatrix} 1 & S_\phi T_\vartheta & C_\phi T_\vartheta \\ 0 & C_\phi & -S_\phi \\ 0 & S_\phi / C_\vartheta & C_\phi / C_\vartheta \end{bmatrix} \boldsymbol{\Omega} = \mathbf{U}\boldsymbol{\Omega}, \tag{1}$$

wherein we use $S_\alpha$, $C_\alpha$ and $T_\alpha$ as shorthand for $\sin\alpha$, $\cos\alpha$ and $\tan\alpha$ respectively. To rotate from the inertial frame to body frame we use the SO(3) matrix

$$\mathbf{R} = \begin{bmatrix} C_\vartheta C_\psi & C_\vartheta S_\psi & -S_\vartheta \\ S_\phi S_\vartheta C_\psi - C_\phi S_\psi & S_\phi S_\vartheta C_\psi + C_\phi C_\psi & S_\phi C_\vartheta \\ C_\phi S_\theta C_\psi + S_\phi S_\psi & C_\phi S_\theta S_\psi - S_\phi C_\psi & C_\phi C_\vartheta \end{bmatrix}.$$

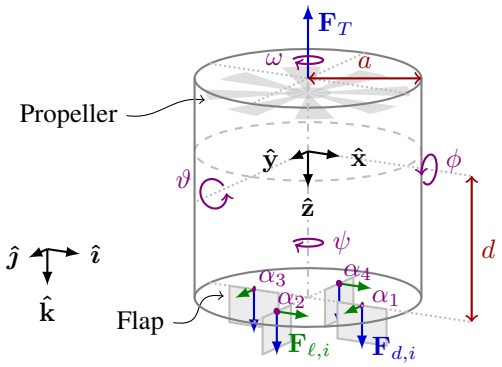


Fig. 1: Sketch of the rigid body physical model for the UAV.

### B. Equations of Motion

Consider a simplified rigid-body physical model sketched in Fig. 1. With respect to the inertial frame the equations of motion from the Newton-Euler formalism are

$$m\ddot{\mathbf{P}} = \mathbf{R}^\mathsf{T}\mathbf{F} \tag{2a}$$

$$\mathbf{J}\dot{\boldsymbol{\Omega}} = -\boldsymbol{\Omega} \times \mathbf{J}\boldsymbol{\Omega} + \boldsymbol{\tau}, \tag{2b}$$

where $m$ is the total mass, $\mathbf{P}$ is the position, $\mathbf{F}$ and $\boldsymbol{\tau}$ the total force and torque in the body frame respectively, and finally $\mathbf{J}$ the moment of inertia, which is assumed to be a diagonal matrix.

In the body frame we model the total force $\mathbf{F}$ acting on the UAV following [5] by considering a thrust force from the ducted-fan $\mathbf{F}_T = -k_T\omega^2\hat{\mathbf{z}}$ as a function of the propeller's angular velocity $\omega$. Because of the geometry we approximate

End term project for course *Robust Control and Convex Optimization* taught by Prof. Dr. R. S. Smith at ETH Zurich. *Student ID: 19-150-903 Email: nproSS@student.ethz.ch. Thanks to T. Rothlin for providing the electromechanical parameters for the UAV.

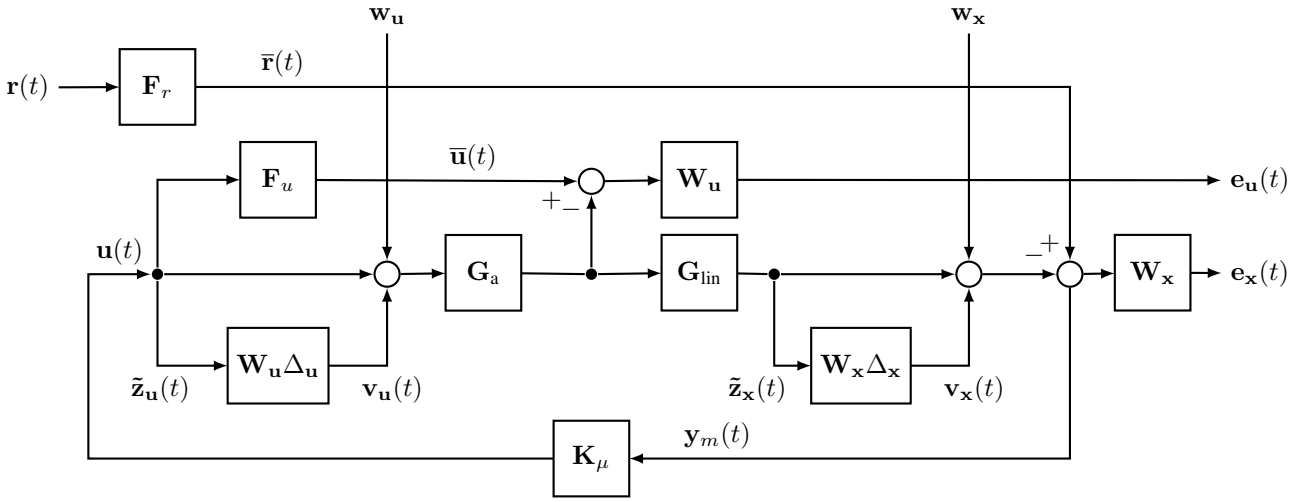


Fig. 2: Closed loop uncertain plant model $\mathcal{L}(\Delta, \mathcal{L}(\mathbf{G}, \mathbf{K}_\mu))$ with weighting functions. For compactness in the block diagram the uncertainty blocks for the actuators have been merged into a single matrix $\Delta_\mathbf{u} = \mathrm{blkdiag}(\Delta_\alpha, \delta_\omega)$. Conversely, the error vector has been partitioned into two components, $\mathbf{e_u} = [\boldsymbol{\alpha}^\mathsf{T}\ \omega]^\mathsf{T}$ and $\mathbf{e_x} = [(\mathbf{r}-\mathbf{y})^\mathsf{T}\ \dot{\mathbf{P}}^\mathsf{T}\ \boldsymbol{\Theta}^\mathsf{T}\ \boldsymbol{\Omega}^\mathsf{T}]^\mathsf{T}$. The block diagram for the nominal plant $\mathbf{G}_\mathrm{nom}$ is obtained by setting $\Delta_\mathbf{u}$ and $\Delta_\mathbf{x}$ to zero.

the generated air velocity field in the duct as being constant and collinear to $\hat{\mathbf{z}}$ [8]

$$\boldsymbol{\nu} = \sqrt{\frac{F_T}{2a\varrho\pi^2}}\hat{\mathbf{z}} = \frac{\omega}{\pi}\sqrt{\frac{k_T}{2a\varrho}}\hat{\mathbf{z}}. \tag{3}$$

The *drag* and *lift* forces generated by the interaction of each flap with the air velocity field are then $\mathbf{F}_d = \frac{1}{2}\varrho S C_d \nu^2 \hat{\mathbf{z}}$ and $\mathbf{F}_\ell = \frac{1}{2}\varrho S C_\ell \nu^2 \hat{\mathbf{n}}$ respectively ($\hat{\mathbf{n}}$ being given by the orientation of the flap). The density of air $\varrho$ is assumed to be constant, while the drag coefficients $S$, $C_d$ and $C_\ell$ depend on the angle of attack $\alpha$ of the flap making them quite difficult to determine. Hereinafter, under the assumption that $\alpha$ is small they will be approximated with $C_d = c_d\alpha^2 + c_0$, $C_\ell = c_\ell\alpha$ [7, 8] and $S$ is considered a constant. Finally, gravity adds a term $\mathbf{F}_g = mg\mathbf{R}^\mathsf{T}\hat{\mathbf{k}}$.

For the total torque it is derived from the geometry that each flap induces $\boldsymbol{\tau}_f = (\frac{1}{3}a\hat{\mathbf{t}} + d\hat{\mathbf{z}}) \times (\mathbf{F}_d + \mathbf{F}_\ell)$, with $\hat{\mathbf{t}} = \hat{\mathbf{n}} \times \hat{\mathbf{z}}$. In addition there is also a torque induced by the gyroscopic procession $\boldsymbol{\tau}_g = \mathbf{R}^\mathsf{T}\omega J_r \hat{\mathbf{k}} \times \boldsymbol{\Omega}$ with $J_r$ being the inertia of the propeller with respect to its spin axis [5]. The resulting total quantities are then

$$\begin{aligned}\mathbf{F} &= mg\mathbf{R}^\mathsf{T}\hat{\mathbf{k}} - k_T\omega^2\hat{\mathbf{z}} \\ &\quad + \frac{\varrho S\nu^2}{2}\sum_i \left(c_d\alpha_i^2 + c_0\right)\hat{\mathbf{z}} + c_\ell\alpha_i\hat{\mathbf{n}}_i, \end{aligned}\tag{4a}$$

$$\boldsymbol{\tau} = \omega J_r \mathbf{R}^\mathsf{T}(\hat{\mathbf{k}} \times \boldsymbol{\Omega}) + \frac{\varrho c_\ell S\nu^2 d}{2}\hat{\mathbf{z}} \times \sum_i \alpha_i\hat{\mathbf{n}}_i. \tag{4b}$$

### C. Linearized Dynamics

To synthesize a controller we simplify the dynamics to a state-space LTI model $\dot{\mathbf{x}} = \mathbf{A}_x\mathbf{x} + \mathbf{B}_{xu}\mathbf{u}$, $\mathbf{y} = \mathbf{C}_{yx}\mathbf{x} + \mathbf{D}_{yu}\mathbf{u}$ with state and inputs given by

$$\mathbf{x} = \begin{bmatrix}\mathbf{P}^\mathsf{T} & \dot{\mathbf{P}}^\mathsf{T} & \boldsymbol{\Theta}^\mathsf{T} & \boldsymbol{\Omega}^\mathsf{T}\end{bmatrix}^\mathsf{T}, \quad \mathbf{u} = \begin{bmatrix}\boldsymbol{\alpha}^\mathsf{T} & \omega\end{bmatrix}^\mathsf{T} \tag{5}$$

respectively. In particular, for the uncertain model presented in a following section, note that the state transition matrix of the linear model is given by a Jacobian with the following structure

$$\mathbf{A}_x = \begin{bmatrix} 0 & \mathbf{I}_3 & 0 & 0 \\ 0 & \frac{1}{m}\mathbf{R}^\mathsf{T}\frac{\partial \mathbf{F}}{\partial \dot{\mathbf{P}}} & \frac{1}{m}\frac{\partial(\mathbf{R}^\mathsf{T}\mathbf{F})}{\partial \boldsymbol{\Theta}} & \frac{1}{m}\mathbf{R}^\mathsf{T}\frac{\partial \mathbf{F}}{\partial \boldsymbol{\Omega}} \\ 0 & 0 & \frac{\partial \mathbf{U}}{\partial \boldsymbol{\Theta}}\boldsymbol{\Omega} & \mathbf{U} \\ 0 & \mathbf{J}^{-1}\frac{\partial \boldsymbol{\tau}}{\partial \dot{\mathbf{P}}} & \mathbf{J}^{-1}\frac{\partial \boldsymbol{\tau}}{\partial \boldsymbol{\Theta}} & \mathbf{J}^{-1}\left[\frac{\partial \boldsymbol{\tau}}{\partial \boldsymbol{\Omega}} - \frac{\partial(\boldsymbol{\Omega}\times\mathbf{J}\boldsymbol{\Omega})}{\partial \boldsymbol{\Omega}}\right] \end{bmatrix}$$

The linearization is performed in a stationary hovering state at height $h$ above the ground and yaw angle of $45°$ or $\mathbf{P}_0 = -h\hat{\mathbf{k}}$, $\boldsymbol{\Theta}_0 = \frac{\pi}{4}\hat{\boldsymbol{\psi}}$, thus $x_0 = [\mathbf{P}_0^\mathsf{T}\ \mathbf{0}^\mathsf{T}\ \boldsymbol{\Theta}_0^\mathsf{T}\ \mathbf{0}^\mathsf{T}]^\mathsf{T}$ and $u_0 = [\mathbf{0}^\mathsf{T}\ \omega_0]^\mathsf{T}$, where $\omega_0 \approx \sqrt{mg/k_T}$ is the propeller's angular velocity to make the UAV hover. Finally, all inputs and outputs are normalized to lie in the range $(-1, 1)$.

### D. State Observer and Actuators

The state is assumed to be known, as there is an inertial measurement unit with a dedicated sensor fusion chip onboard [1]. Thus, we only need to model a measurement delay $T_m$ and the actuators. The linearized dynamics are extended with 3nd order Padé approximant $G_m(s) \approx e^{-sT_m}$ for the output delay and two transfer functions $G_\alpha(s)$, $G_\omega(s)$ for the flaps and thruster respectively. Specifically, $G_\alpha(s)$ is a critically damped 2nd order low pass filter (LPF), while $G_\omega(s)$ is a first order LPF. The MIMO diagonal transfer function for the actuators is then given by scaling the transfer functions by the number of actuators:

$$\mathbf{G}_\mathrm{a}(s) = \begin{bmatrix} G_\alpha(s)\mathbf{I}_4 & \\ & G_\omega(s)) \end{bmatrix}. \tag{6}$$

### E. Generalized Uncertain Plant Model

Because of the simplified aerodynamics modelling and the linearization procedure, the resulting controller may be un-

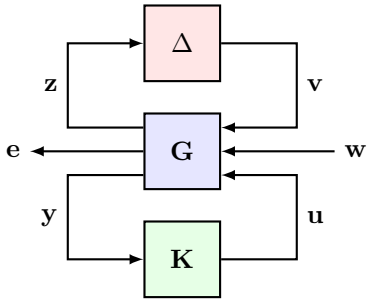


Fig. 3: Generalized plant structure.

aware of large errors. Hence, to compensate for this fact both sources of inaccuracy are addressed by introducing uncertain block elements using the *generalized plant* and *structured singular value* (SSV) techniques presented in [9, 10]. For the present application, we define the class of uncertainty using the full block diagonal matrices from the set

$$\mathbf{\Delta} = \left\{ \begin{bmatrix} \Delta_\alpha & & \\ & \delta_\omega & \\ & & \Delta_{\mathbf{x}} \end{bmatrix} \;\middle|\; \begin{matrix} \Delta_\alpha \in \mathbb{C}^{4\times 4}, \delta_\omega \in \mathbb{C}, \\ \Delta_{\mathbf{x}} \in \mathbb{C}^{9\times 9} \end{matrix} \right\}, \tag{7}$$

where $\Delta_\alpha$ models the errors in the flap aerodynamics, $\Delta_\omega$ propeller aerodynamics and $\Delta_{\mathbf{x}}$ compensates the error caused by linearization. Because of the aforementioned special structure of the Jacobian in the previous section, the size of $\Delta_{\mathbf{x}}$ can reduced to be 9 dimensional instead of 12 as the dynamics of in the position are already linear in the state.

The uncertain blocks are then added around the linearized plant $\mathbf{G}_{\text{lin}}$ of the previous sections as percentage error uncertainties as shown in Fig. 2. The other weighting and filtering blocks in the diagram will be discussed in the next section. Finally the plant is brought in the form shown in Fig. 3 and partitioned accordingly to obtain

$$\begin{bmatrix} \mathbf{z} \\ \mathbf{e} \\ \mathbf{y}_m \end{bmatrix} = \begin{bmatrix} \mathbf{A}_{zv} & \mathbf{B}_w & \mathbf{B}_u \\ \mathbf{C}_e & \mathbf{D}_{ew} & \mathbf{D}_{eu} \\ \mathbf{C}_y & \mathbf{D}_{yw} & \mathbf{D}_{yu} \end{bmatrix} \begin{bmatrix} \mathbf{v} \\ \mathbf{w} \\ \mathbf{u} \end{bmatrix} = \mathbf{G} \begin{bmatrix} \mathbf{v} \\ \mathbf{w} \\ \mathbf{u} \end{bmatrix}. \tag{8}$$

From the diagram one can retrieve that the signals are control inputs $\mathbf{u} \in \mathbb{R}^5$, exogenous inputs $\mathbf{w} = [\mathbf{w}_\alpha^\mathsf{T}\ \mathbf{r}^\mathsf{T}]^\mathsf{T} \in \mathbb{R}^7$, nominal outputs (measurements) $\mathbf{y}_m = [(\mathbf{r}-\mathbf{y})^\mathsf{T}\ \dot{\mathbf{P}}^\mathsf{T}\ \mathbf{\Theta}^\mathsf{T}\ \mathbf{\Omega}^\mathsf{T}]^\mathsf{T}$ and errors $\mathbf{e} = [\boldsymbol{\alpha}^\mathsf{T}\ \omega\ (\mathbf{r}-\mathbf{y})^\mathsf{T}\ \dot{\mathbf{P}}^\mathsf{T}\ \mathbf{\Theta}^\mathsf{T}]^\mathsf{T}$.

## III. Controller Design

### A. Control Problem

The control objective is to track a piecewise constant position reference $\mathbf{r}(t) \in \mathbb{R}^3$ in the inertial frame. The controller should move the UAV to $\mathbf{r}(t)$ with control actions that do not exceed the actuator limits $\alpha \in (\underline{\alpha}, \overline{\alpha})$, $\omega \in [0, \overline{\omega})$, do not bring the angular components of the state too far from their set point, i.e. $\mathbf{\Theta} \in (-\varphi, \varphi)^3$, and do not exceed the velocity limits $\|\dot{\mathbf{P}}\|_1 \leq \overline{v}$.

### B. Weighting Functions

In order to tune the control objective function several weighting functions are introduced. For the reference $\mathbf{r}(t)$ and nominal inputs $\mathbf{u}$ there are two second order filters $\mathbf{F_r}$ and $\mathbf{F_u}$ respectively. The two provide desirable step responses to track, for the entire device with $\mathbf{F_r}$ and for the actuators with the latter:

$$\mathbf{F_u} = \begin{bmatrix} \dfrac{\mathbf{I}_4}{T_\alpha s + 1} & \\ & \dfrac{1}{T_\omega s + 1} \end{bmatrix}, \tag{9a}$$

$$\mathbf{F_r} = \begin{bmatrix} \dfrac{\mathbf{I}_2}{T_{xy}^2 s^2 + 2T_{xy} s + 1} & \\ & \dfrac{1}{T_z^2 s^2 + 2T_z s + 1} \end{bmatrix}, \tag{9b}$$

with $T_\alpha \approx 0.13\,\text{s}, T_\omega \approx 0.1\,\text{s}, T_{xy} = T_z \approx 6\,\text{s}$.

The other weighting functions for the $\mathcal{H}_\infty$ design, as well as the uncertainty weights for the μ-synthesis are shown in Fig. 4a. Because the horizontal and vertical axis use different actuators, flaps and propeller respectively, the performance weights for position and velocity have been split into $x, y$ and $z$ components. Similarly, because rotations along the yaw axis are less relevant for stability the Euler angles weights have been separated into two groups $\phi, \vartheta$ and $\psi$.

Finally, the uncertainty weighting functions are derived from the percentage uncertainty of some electrical or mechanical parameters. As these are internal to the system dynamics, they need to be converted into equivalent input uncertainty errors. Considering the parameters $S, c_d, c_\ell, k_T, J_r$ and defining a percentage error $\varepsilon_S, \varepsilon_d, \varepsilon_\ell, \varepsilon_T, \varepsilon_r$ for each with respect to a nominal value it is possible to derive an (upper bound) of an equivalent input error composed by

$$\varepsilon_\omega = \max\left(\frac{\varepsilon_T}{2}, \varepsilon_r\right) \tag{10a}$$

$$\varepsilon_\alpha = \max\left((\varepsilon_\ell + \varepsilon_S + 2\varepsilon_\omega), (\varepsilon_S + \varepsilon_d + \varepsilon_\omega)\right) \tag{10b}$$

With regards to the state linearization error, it is assumed that it remains below 20% at all time during the flight envelope and is decreasing but not vanishing at lower frequencies.

### C. $\mathcal{H}_\infty$ Synthesis

To perform $\mathcal{H}_\infty$ the nominal plant (without uncertainties) is taken with the aforementioned performance functions yielding a plat of the form

$$\begin{bmatrix} \mathbf{e} \\ \mathbf{y}_m \end{bmatrix} = \begin{bmatrix} \mathbf{D}_{ew} & \mathbf{D}_{eu} \\ \mathbf{D}_{yw} & \mathbf{D}_{yu} \end{bmatrix} \begin{bmatrix} \mathbf{w} \\ \mathbf{u} \end{bmatrix} = \mathbf{G}_{\text{nom}} \begin{bmatrix} \mathbf{w} \\ \mathbf{u} \end{bmatrix}. \tag{11}$$

The $\mathcal{H}_\infty$ synthesis is then performed using the Riccati method yielding a stable controller $\mathbf{K}_\infty$ with $\gamma = \|\mathcal{L}(\mathbf{G}_{\text{nom}}, \mathbf{K}_\infty)\|_\infty \approx 0.6$. Here we used the notation $\mathcal{L}$ for the linear fractional transformation interconnection.

### D. μ-Synthesis with $DK$-iteration

In order to obtain a more robust design, we then proceed with the $DK$-iteration method as shown in [10]. The iteration finds the solution to the problem

$$\mathbf{K}_\mu = \arg\min_{\mathbf{K}} \inf_{\mathbf{D}\in\mathcal{D}} \|\mathbf{D}\mathcal{L}(\mathbf{G}, \mathbf{K})\mathbf{D}^{-1}\|_\infty, \tag{12}$$

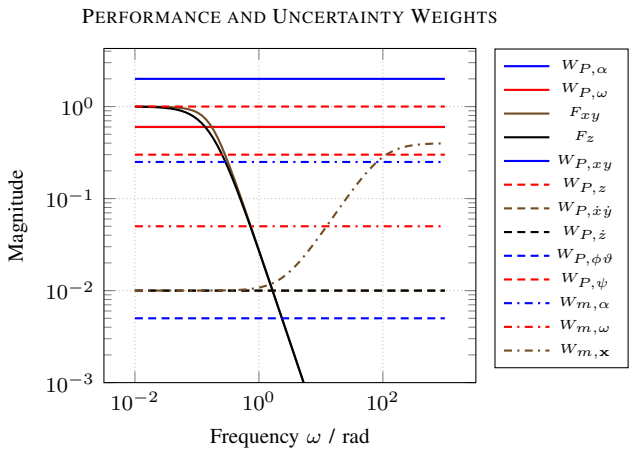


(a) Weighting functions for $\mathcal{H}_\infty$ and μ-synthesis designs. Since there are already filters to track certain desired step responses most of the weights are scalar.

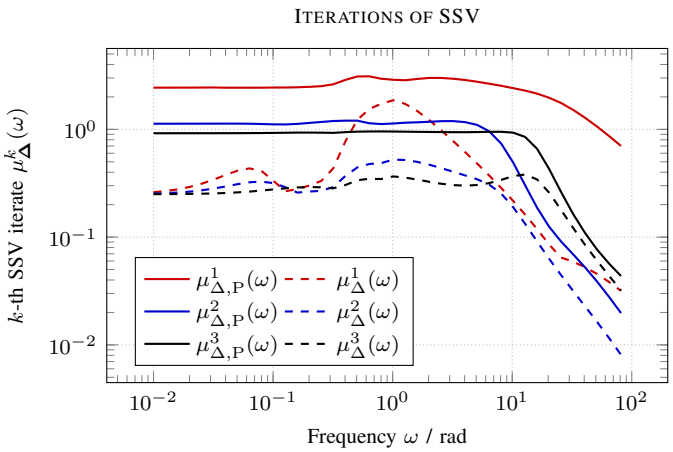


(b) Change in the SSV during the $DK$-iteration. Dashed lines are the SSV for robust stability, while the solid line of the corresponding color is the robust performance SSV.

Fig. 4: $\mathcal{H}_\infty$ weights and SSV during the $DK$-iteration.

by repeatedly solving one of the two minimizations while keeping the other fixed [9, 10]. The following version of the algorithm was implemented using MATLAB's Robust Control Toolbox.

**function** DKITER($\mathbf{G}$, $\mathbf{K}_\infty$)
  $\mathbf{K}_\mu \leftarrow \mathbf{K}_\infty$ ▷ *Initialize with nominal* $\mathcal{H}_\infty$.
  **repeat**
    ▷ *Find an upper bound "scaling" in the frequency domain, keep* $\mathbf{K}_\mu$ *fixed* ◁
    $\mathbf{D}(i\omega) \leftarrow \arg\inf_{\tilde{\mathbf{D}}(i\omega)} \overline{\sigma}(\tilde{\mathbf{D}}\mathcal{L}(\mathbf{G},\mathbf{K}_\mu)\tilde{\mathbf{D}}^{-1})$
    ▷ *Approximate the scaling with a minimum phase transfer function* ◁
    Fit $\hat{\mathbf{D}}(s)$ so that $\forall\omega : |\hat{\mathbf{D}}(i\omega)| \approx \mathbf{D}(i\omega)$
    ▷ *Synthesize an* $\mathcal{H}_\infty$ *controller, keep* $\mathbf{D}$ *fixed* ◁
    $\mathbf{K}_\mu \leftarrow \arg\min_{\tilde{\mathbf{K}}} \|\hat{\mathbf{D}}\mathcal{L}(\mathbf{G},\tilde{\mathbf{K}})\hat{\mathbf{D}}^{-1}\|_\infty$
  **until** $\mu_{\tilde{\mathbf{\Delta}}}(\mathcal{L}(\mathbf{G},\mathbf{K}_\mu)) < 1$
  **return** $\mathbf{K}_\mu$

In the listing above the SSV was computed on the augmented perturbation set

$$\tilde{\mathbf{\Delta}} = \left\{ \begin{bmatrix} \Delta & \\ & \Delta_P \end{bmatrix} \,\middle|\, \Delta \in \mathbf{\Delta}, \Delta_P \in \mathbb{C}^{5\times 12} \right\} \tag{13}$$

in order to make use of the main loop theorem from [9]. Hence the set of scaling matrices that commute with elements of $\tilde{\mathbf{\Delta}}$ is

$$\mathcal{D} = \left\{ \begin{bmatrix} d_\alpha \mathbf{I}_4 & & & \\ & d_\omega & & \\ & & d_{\mathbf{x}}\mathbf{I}_9 & \\ & & & d_P\mathbf{I}_n \end{bmatrix} \,\middle|\, \begin{matrix} d_\alpha, d_\omega, \\ d_{\mathbf{x}}, d_P \in \mathbb{C} \end{matrix} \right\}, \tag{14}$$

where $n$ is 12 for the left scales and 5 for the right (inverse) scaling matrices. The iteration took 3 steps to converge to a solution resulting in the sequence of SSV iterates shown in Fig. 4b.

## IV. Simulation and Results

The nominal closed loop plants for both controllers, that is $\mathbf{G}_{\mathrm{cl},\infty} = \mathcal{L}(\mathbf{G},\mathbf{K}_\infty)$ $\mathbf{G}_{\mathrm{cl},\mu} = \mathcal{L}(\mathbf{G},\mathbf{K}_\mu)$ for $\mathcal{H}_\infty$ and μ-synthesis respectively, were tested with a simulation of a step response of $50\,\mathrm{cm}$ along the $x$. Both controllers track the reference taking around 20 seconds to perform the maneuver. The results are plotted in Fig. 5 and Fig. 6.

## References

[1] T. Rothlin, "Optimization of a ducted fan prototype," Semester Project, OST RJ University of Applied Sciences, Rapperswil, Switzerland, 2024. [Online]. Available: https://www.ost.ch/de/details/abstracts/optimization-of-a-ducted-fan-prototype-18926.

[2] T. Rothlin and T. Tönz, "Flight control system for hovering a 'ducted-fan' prototype," Bachelor Thesis, OST RJ University of Applied Sciences, Rapperswil, Switzerland, 2021, 114 pp. [Online]. Available: https://www.ost.ch/de/details/abstracts/ducted-fan-prototype-17443.

[3] J. Pflimlin, P. Soueres, and T. Hamel, "Hovering flight stabilization in wind gusts for ducted fan UAV," in *2004 43rd IEEE Conference on Decision and Control (CDC) (IEEE Cat. No.04CH37601)*, Nassau, Bahamas: IEEE, 2004, 3491–3496 Vol.4, ISBN: 978-0-7803-8682-2. DOI: 10.1109/CDC.2004.1429251. [Online]. Available: http://ieeexplore.ieee.org/document/1429251/ (visited on 03/25/2024).

[4] J.-M. Pflimlin, P. Binetti, P. Souères, T. Hamel, and D. Trouchet, "Modeling and attitude control analysis of a ducted-fan micro aerial vehicle," *Control Engineering Practice*, vol. 18, no. 3, pp. 209–218, Mar. 2010, ISSN: 09670661. DOI: 10.1016/j.conengprac.2009.09.009. [Online]. Available: https://linkinghub.elsevier.com/retrieve/pii/S0967066109001828 (visited on 03/25/2024).

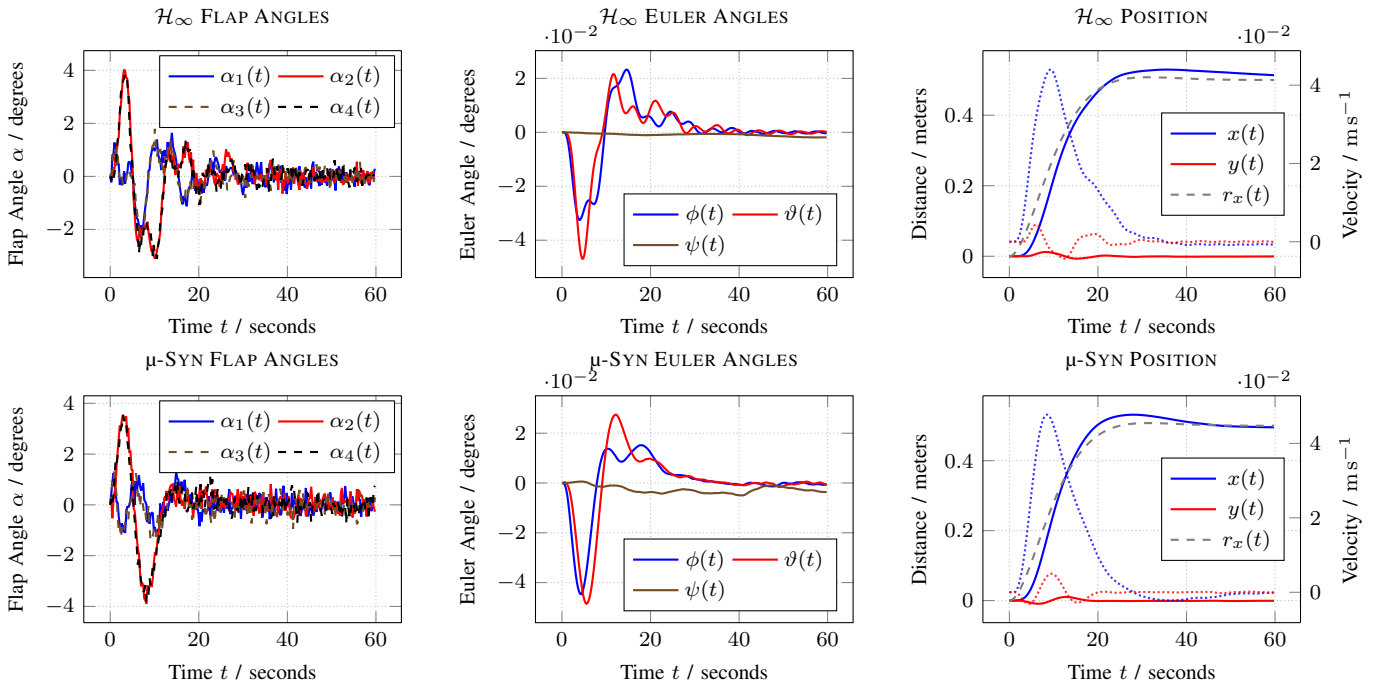


Fig. 5: Simulated step responses along $x$ of the closed loop nominal $\mathcal{H}_\infty$ and μ-synthesis controller designs. In the rightmost plots, continuous lines show the position error while dotted lines with the right axis are the velocity in the corresponding directions. The dashed line for $r_x(x)$ is the filtered reference that is tracked by the controllers.

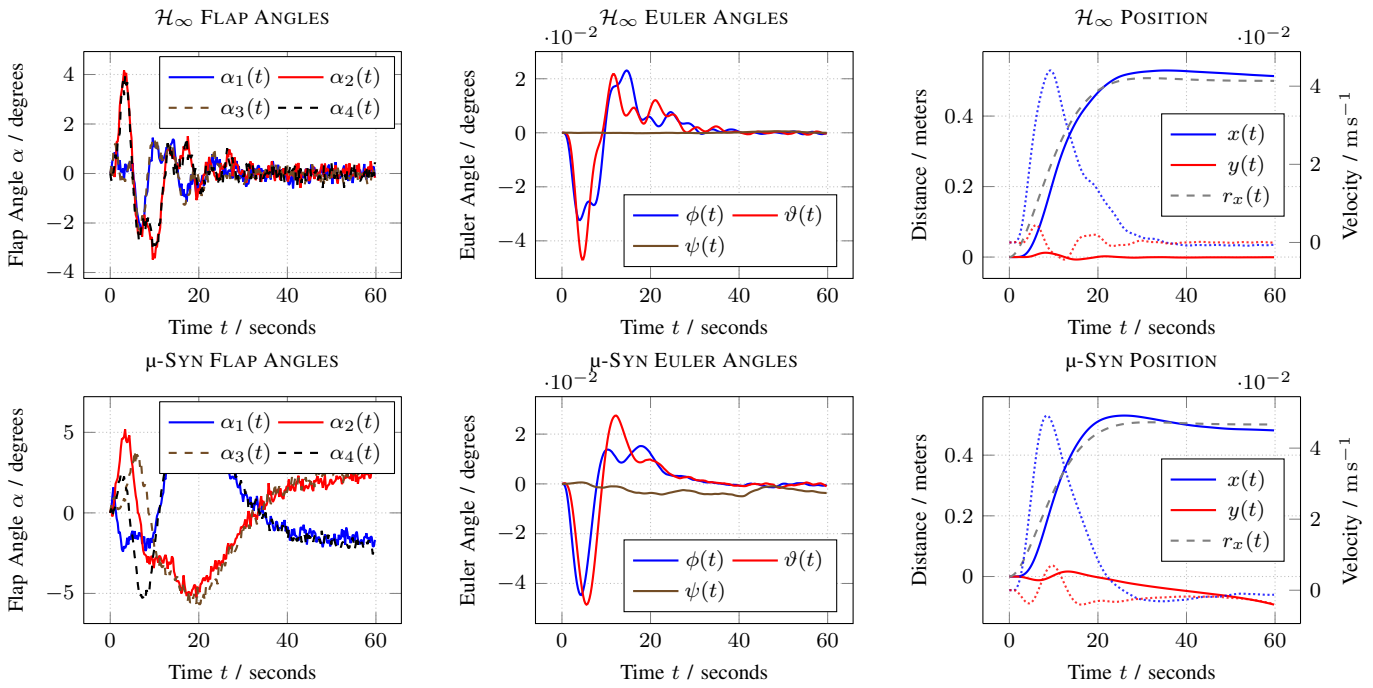


Fig. 6: Simulated step responses along $x$ of the closed loop perturbed $\mathcal{H}_\infty$ and μ-synthesis controller designs. In the rightmost plots, continuous lines show the position error while dotted lines with the right axis are the velocity in the corresponding directions. The dashed line for $r_x(x)$ is the filtered reference that is tracked by the controllers.

[5] R. Naldi, L. Gentili, L. Marconi, and A. Sala, "Design and experimental validation of a nonlinear control law for a ducted-fan miniature aerial vehicle," *Control Engineering Practice*, vol. 18, no. 7, pp. 747–760, Jul. 2010, ISSN: 09670661. DOI: 10.1016/j.conengprac.2010.02.007. [Online]. Available: https://linkinghub.elsevier.com/retrieve/pii/S0967066110000444 (visited on 03/26/2024).

[6] G. Avanzini, G. De Matteis, and F. Fresta, "Robust multivariable control of a shrouded-fan uninhabited aerial vehicle," in *AIAA Atmospheric Flight Mechanics Conference and Exhibit*, Monterey, California: American Institute of Aeronautics and Astronautics, Aug. 5, 2002, ISBN: 978-1-62410-107-6. DOI: 10.2514/6.2002-4703. [Online]. Available: https://arc.aiaa.org/doi/10.2514/6.2002-4703 (visited on 05/29/2024).

[7] R. F. Stengel, *Flight dynamics*, Second edition. Princeton Oxford: Princeton University Press, 2022, 894 pp., ISBN: 978-0-691-22025-3.

[8] J. L. Pereira, "Hover and wind-tunnel testing of shrouded rotors for improved micro air vehicle design," Ph.D. dissertation, University of Maryland (College Park, Md.), Aug. 29, 2008. [Online]. Available: http://hdl.handle.net/1903/8752 (visited on 03/31/2024).

[9] A. Packard and J. Doyle, "The complex structured singular value," *Automatica*, vol. 29, no. 1, pp. 71–109, Jan. 1993, ISSN: 00051098. DOI: 10.1016/0005-1098(93)90175-S. [Online]. Available: https://linkinghub.elsevier.com/retrieve/pii/000510989390175S (visited on 03/31/2024).

[10] S. Skogestad and I. Postlethwaite, *Multivariable feedback control: analysis and design*, 2. ed., repr. Chichester: Wiley, 2010, 574 pp., ISBN: 978-0-470-01168-3 978-0-470-01167-6.